Int J Clin Exp Pathol 2011;4(1):43-57
www.ijcep.com /IJCEP1012004

Original Article

Phenotypic variations in NF1-associated low grade astrocytomas: possible role for increased mTOR activation in a subset

Mark Jentoft[1], Caterina Giannini[1], Ling Cen[2], Bernd W. Scheithauer[1], Bridget Hoesley[3], Jann N. Sarkaria[2], Patrice C. Abell-Aleff[4], Erika F. Rodriguez[1], Ying Li[5], Fausto J. Rodriguez[1,6]

[1]Departments of Laboratory Medicine and Pathology, [2]Radiation Oncology, [3]Advanced Genomics Technology Center, [4]Biochemistry and Molecular Biology, [5]Biomedical Statistics and Informatics, Mayo Clinic, Rochester, MN, USA; [6]Department of Pathology, Johns Hopkins University, Baltimore, MD, USA.

Received December 7, 2010; accepted December 11, 2010; Epub December 12, 2010; published January 1, 2011

Abstract: Low grade astrocytomas are the most common CNS tumors in neurofibromatosis type 1(NF1) patients. While most are classic pilocytic astrocytomas (PA), some are difficult to classify, and have been termed "low grade astrocytoma subtype indeterminate" (LGSI). Some of these tumors exhibit peculiar morphologies, including plump cytoplasmic processes and macronucleoli. In the current study we performed electron microscopy, followed by gene expression, immunohistochemical and western blot analyses in an effort to identify biological differences underlying phenotypic variation in NF1-associated low grade astrocytoma. Electron microscopy demonstrated intermediate filaments and frequent Rosenthal fiber material in both PA and LGSI. Dense core granules and/or aligned microtubules were present in the LGSI group (2 of 3 cases) and in the PA group (1 of 10 cases). Analysis of global gene expression data obtained using Affymetrix HG-U133 Plus2.0 chips (5 PA, 1 LGSI), and western blot analysis for phospho-S6 (1 LGSI, 2 PA) demonstrated a gene expression profile reflecting "neuronal differentiation" and increased phospho-S6 immunoreactivity consistent with mTOR activation in the LGSI compared with PA. These findings were confirmed by immunohistochemistry for neuronal markers, as well as combined phospho-S6/ phospho-p70S6K immunoreactivity in 4 (of 4) LGSI vs. 5 (of 13) NF1-associated PA (p=0.02), and 13 (of 39) sporadic PA. Phospho-ERK immunoreactivity was uniformly present in PA and LGSI groups, while *BRAF* duplication was absent by FISH in 8 NF1-associated low grade astrocytomas. In summary, differential expression of neuronal-related genes and increased mTOR activation may underlie phenotypic variations in NF1-associated low grade astrocytomas.

Keywords: Neurofibromatosis, glioma, astrocytoma, pilocytic astrocytoma, mTOR, glioneuronal

Introduction

Neurofibromatosis type 1 (NF1) patients show a predisposition to the formation of both peripheral and central nervous system (CNS) tumors. While most NF1-associated CNS neoplasms are low grade astrocytomas with classic features of pilocytic astrocytoma (PA) (49%), a subset remain difficult to classify past the simple designation "low grade astrocytoma subtype indeterminate" (LGSI) (17%) despite detailed histologic examination [1]. No statistically significant differences were noted between the two groups when comparing mitotic activity, MIB-1 labeling indices, p53 labeling indices, degree of microscopic infiltration, time to recurrence after surgery, radiographic progression, or overall disease-specific survival times [1]. It is unknown what relationship LGSI tumors have to PA in this syndromic setting. A curious morphologic variation within LGSI and some PA is the presence of tumors wherein the astrocytic cells feature plump, abundant cytoplasm, thick processes, and central nuclei with prominent nucleoli. Characterization of these phenotypic variations within NF1 is lacking in the literature.

Ultrastructural studies of NF1 related intracranial astrocytomas are few with exception of ones focusing upon optic nerve gliomas [2-5]. A

recent, detailed study of optic gliomas arising in a mouse model of NF1 (*Nf1+/-*^{GFAP}CKO) demonstrated axonal irregularities and glial disorganization at the ultrastructural level associated with retinal ganglion cell loss [6]. Ultrastructurally, conventional PA are characterized by conspicuous intermediate filaments within their piloid cell element, electrondense Rosenthal fiber material, amorphous spheres (hyaline droplets), and accumulation of large cytoplasmic lysosomes (granular bodies) [2, 7]. Ultrastructural properties of the full spectrum of NF1 -associated low grade astrocytomas are not well characterized to our knowledge.

NF1 deficient astrocytes exhibit increased levels of the mammalian target of rapamycin (mTOR) activation, resulting in ribosomal S6 activation in both NF1 mutant murine optic gliomas and NF1 associated pilocytic astrocytomas in humans [8]. mTOR is a nutrient-sensor control protein that signals several translational factors in response to nutrient availability. Additionally, mTOR regulates the rate at which the translational machinery is synthesized, both at the level of transcription and translation as well as serving several other known cellular functions [9]. Activation of mTOR leads to phosphorylation of S6 kinase and activation of ribosomal S6 [8], with identification of phosphorylated S6 kinase or ribosomal S6 serving as surrogates of mTOR activation.

The purpose of this study was to explore phenotypic differences between different subsets of NF1-associated low grade astrocytomas, and understand what molecular differences underlie them. Since some NF1-associated LGSI tumors are morphologically reminiscent of subependymal giant cell astrocytoma (SEGA), a tumor typical of tuberous sclerosis, the molecular hallmark of which is mTOR activation through mutations of the *TSC1* and *TSC2* genes [10], we hypothesized that differential mTOR activation may underlie the phenotypic variation of other low grade astrocytomas in NF1.

Materials and methods

Patients and tumor samples

Detailed clinicopathologic features of these tumors were reported in a prior study [1]. The current study included 22 cases of NF1-associated low grade astrocytomas (16 PA, 6 LGSI, 1 WHO grade II diffuse astrocytoma). A single ganglioglioma was also included. Six of the NF1-associated PA, as well as 39 sporadic PA, --- present on a tissue microarray were also used for phospho-specific antibody immunohistochemistry. All studies were approved by the Institutional Review Board and Biospecimen committee at Mayo Clinic.

Electron microscopy

Fifteen cases with available glutaraldehyde-fixed and Epon embedded material were studied. The sections were stained with uranyl acetate and lead citrate and examined on a Tecnai 12 model transmission electron microscope (FEI Corp., Eindhoven, Netherlands). All tumors were examined for the presence of intermediate filaments, Rosenthal fibers, microtubules, dense core granules, cytoplasmic organelles, and macronucleoli by three neuropathologists (CG, FJR BWS).

Gene expression analysis

RNA gene expression data were analyzed from 6 NF1-associated low grade astrocytomas obtained from a prior single hybridization experiment [11] using Affymetrix HG-U133 Plus 2.0 chips. Upon review of all histologic slides, one tumor had the morphologic features described above (i.e. abundant cytoplasm, prominent nucleoli, scant to absent eosinophilic granular bodies and Rosenthal fibers) and was classified as LGSI. In brief, a standard in-house MicroArray PreProcessing (MAPP) workflow was used to preprocess the data, including BG Correction, normalization and PM correction. Gene expression differences were expressed in the form of fold changes between 1 LGSI and the 5 PA.

Immunohistochemistry

All immunohistochemical studies were performed using a Dako autostainer and the Dual Link Envision detection system, on 5 micron thick formalin-fixed paraffin-embedded, conventional whole sections or tissue microarray sections using antibodies directed against (GFAP) (polyclonal, 1:4000; Dako, Carpinteria, Calif), S –100 protein (polyclonal, 1:1600; Dako), chromogranin A (LK2H10, 1:500; Chemicon, Billerica, Mass), synaptophysin (clone SY38, 1:40; ICN, Costa Mesa, Calif), neurofilament protein (clone 2F11, 1:75; Dako); phospho-ERK (Rabbit

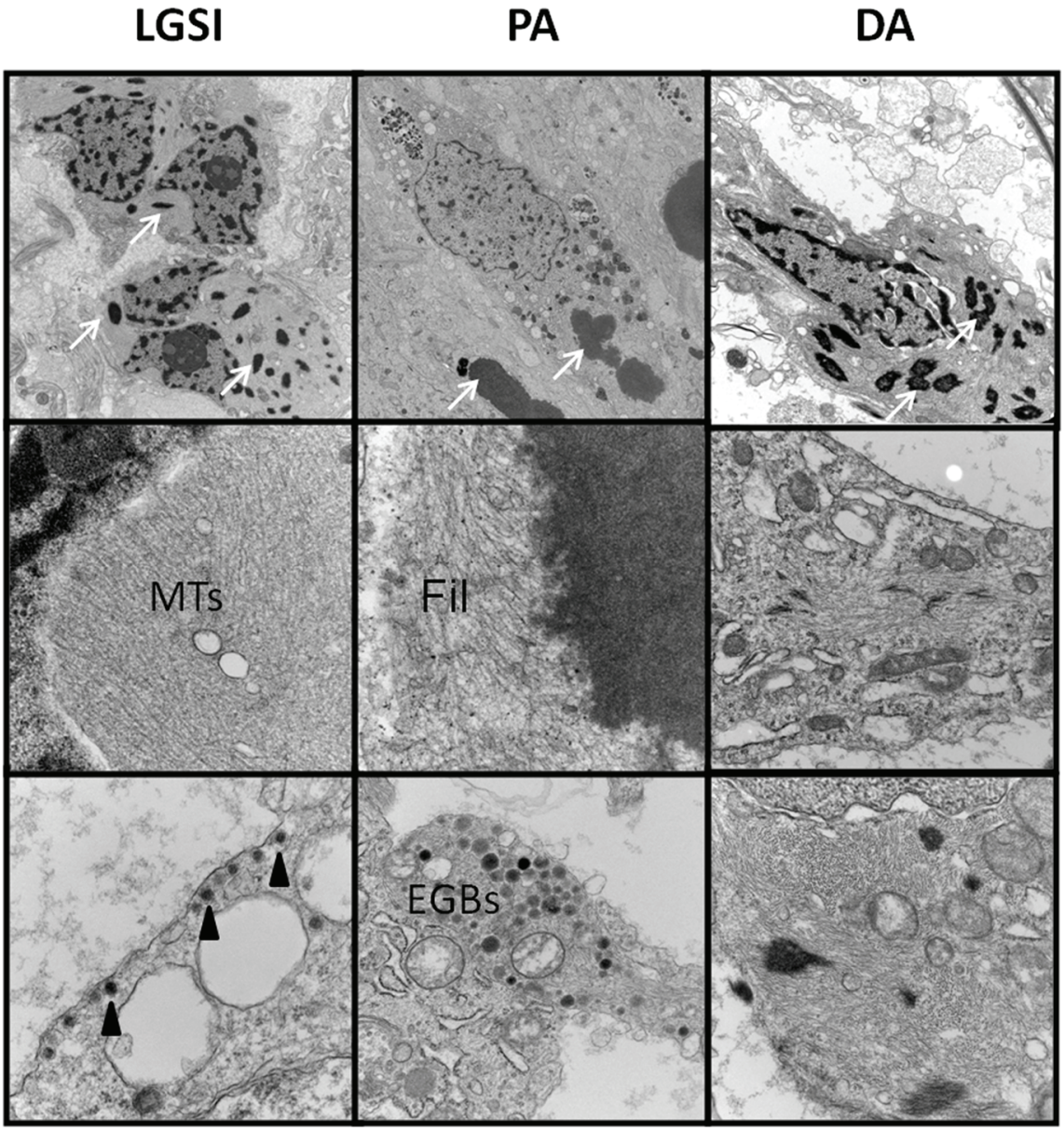

Figure 1. Low grade astrocytomas subtype indeterminate (LGSI) demonstrate ultrastructural features of glial as well as neuronal differentiation. LGSI tumors demonstrated conventional features of glial differentiation including glial intermediate filaments and electrodense Rosenthal fiber material. In addition aligned microtubules and dense core granules were present, consistent with partial neuronal differentiation. Ultrastructural characteristics of neuronal differentiation were infrequent in conventional pilocytic astrocytomas (PA) and absent in the diffuse astrocytoma (DA). Curiously, the latter also showed conspicuous intracytoplasmic Rosenthal fiber material (arrows: Rosenthal fiber material; arrowheads: dense core granules; EGB: eosinophilic granular bodies, Fil=intermediate filaments; MTs: aligned microtubules).

polyclonal(Erk1/2) (Thr202/Tyr204; 1:250 cell signaling technology), phospho-p70S6K (Phospho-p70 S6 Kinase) (Rabbit polyclonal recognizing phospho-Thr389; 1:25; cell signaling technology), phospho-S6 (Rabbit polyclonal p-S6 (Ser235/236) 1:200, cell signaling technology), and Ki–67 (clone MIB-1, monoclonal, 1:300; Dako). Stains were scored according to a four tiered semiquantitative scale by two observers as previously described [11]. MIB-1 (Ki-

67) labeling indices were evaluated using the CAS200 imaging system (Bacus Laboratories, Lombard, Ill) and by examining 20 consecutive high magnification fields.

Western Blot

Total proteins were isolated from patient frozen tissues and separated by 10% SDS-polyacrylamide gel and transferred onto a PVDF membrane. The membrane was blotted overnight at 4 ºC with 1:1000 dilution of primary antibody. Antibodies used were specific for phospho-S6 (Ser235/236), total S6, and β-actin (all from Cell Signaling Technology). Next, the blot was incubated with 1:5000 dilution of secondary anti-rabbit antibody conjugated with horseradish peroxidase (Pierce). Detection was performed with the Super Signal Chemiluminescence reagent according to the manufacturer's protocol (Pierce). Relative quantification of protein levels from western blot bands was done using ImageJ software from the National Institutes of Health (http://rsb.info.nih.gov/ij/index.html).

BRAF fluorescence in situ hybridization (FISH)

FISH studies to evaluate for *BRAF* duplication, a molecular finding characteristic of the majority of sporadic PA, was performed using a custom made probe (clones RP4-592P3, RP4-726N20, RP5-839B19, RP4-813F11), targeting 7q34). The probe was labeled with SpectrumOrange^{tm} (Abbott Molecular/Vysis,Des Plaines, Ill), and a CEP7 control probe was labeled with SpectrumGreen^{tm}. A total of 100 nuclei were evaluated per case. Target to control probe ratios>1.2 were considered indicative of duplication.

Results

Ultrastructural features of NF1-associated low grade astrocytomas

The 14 NF1 associated astrocytomas included 10 PA, 3 LGSI and 1 DA. One NF1 associated GG was also examined. Patients included 6 females and 9 males; mean age at time of surgery was 20 years (range 2-44). Ultrastructural findings are summarized in **Table 1** and illustrated in **Figure 1**. Aligned, often compacted, intermediate filaments typical of astrocytic neoplasms were identified in all tumors, including glial cells of the single GG. Dense core granules were present in the GG and 3(of 3) LGSI. Granules ranged from 100-130 nm in diameter, featured cores of uniform electron density, a surrounding halo, and a sharply delimited membrane. Rosenthal fibers were identified in 4 (of 10) PA. Interestingly, Rosenthal fibers, not evident at the light microscopic level, were seen ultrastructurally in the single diffuse astrocytoma and in 2(of 3) LGSI. Aligned microtubules were identified in 2 (of 3) LGSI. Macronucleoli were identified in 4 (of 10) PA, the single GG, and 2 (of 3) LGSI. Eosinophilic granular bodies were identified in 2 (of 10) PA, the single GG, and in 2 (of 3) LGSI.

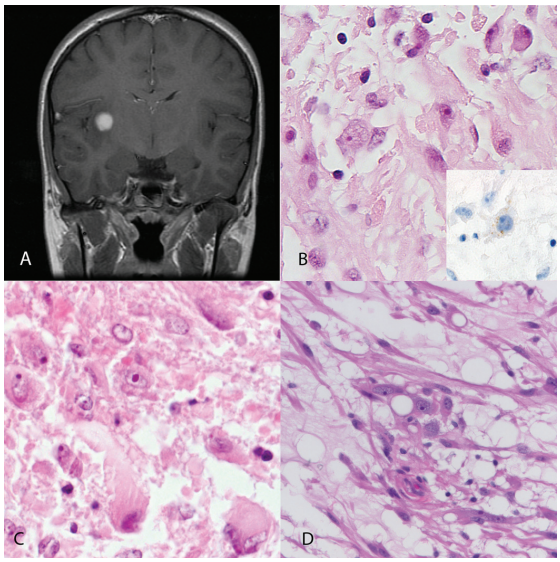

Figure 2. A subset of NF1-associated low grade astrocytomas show distinctive morphology. The subset of low grade astrocytomas characterized by plump processes and macronucleoli had a predilection for the supratentorial brain hemispheres, where they formed well circumscribed masses (A). Corresponding histology (B), a tumor that also expressed chromogranin A in isolated cells (inset). Another example of LGSI (case used for gene expression and Western Blot studies in **figure 4** and **table 3**)(C). These tumors demonstrated some overlap with pilocytic astrocytoma, including the presence of elongated bipolar cells in a loose textured background (D), but lacked Rosenthal fibers at the H&E level in all instances, and eosinophilic granular bodies in most.

A subset of NF1-associated low grade astrocytomas are characterized by unique cytology

In a prior study we described a subset of low grade NF1-associated astrocytomas that dem-

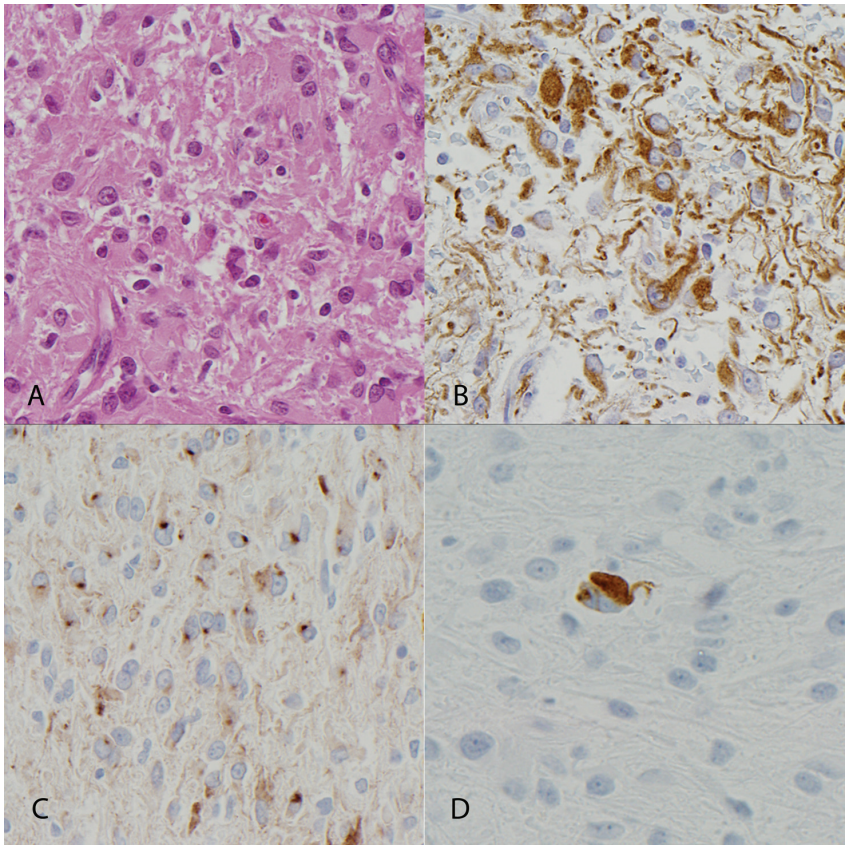

Figure 3. Low grade astrocytomas subtype indeterminate (LGSI) express neuronal associated proteins. A subset of LGSI show peculiar morphologic features including plump, eosinophilic cytoplasmic processes and macronucleoli (A) (H&E). Strong expression of GFAP was noted in all tumors (B). Synaptophysin immunoreactivity, sometimes in a paranuclear pattern in addition to cytoplasmic/cell surface pattern, was noted in half of the cases tested (C). Immunoreactivity for neurofilament protein in isolated cells was also a feature of synaptophysin expressing tumors (D).

onstrated some morphologic features of PA, but in addition had unique cytology [1]. Clinicopathologic features of the tumors evaluated in the current study are summarized in **Table 2.** In summary, these tumors had some features reminiscent of PA, including relative circumscription, hyalinized/glomeruloid vasculature, a loose texture, and bipolar processes in a subset of cells. However, they were characterized cytologically by abundant eosinophilic cytoplasm and prominent nucleoli (**Figure 2**). Rosenthal fibers were absent, as well as eosinophilic granular bodies except for one case. In addition, they were predominantly supratentorial (5 of 6 cases), and mostly situated in the cerebral hemispheres (4 of 6 cases), unlike NF1-associated PA, of which 5 (of 10) involved the optic pathways or brainstem (**Table 1**).

A subset of NF1-associated low grade astrocytomas show a partial neuronal phenotype

We compared changes in global mRNA gene expression between 1 LGSI with the cytologic traits described above and 5 PA. A total of 9035 transcripts were differentially expressed between the LGSI and the PAs. The top overexpressed genes in the LGSI were enriched for neuronal specific genes, including ones encoding proteins associated with synapses, microtubules, secretory granules and neurotransmitters (**Table 3**). Of note the top 3 genes with increased expression were GABA A receptor, synaptotagmin 1, and neurogranin which are all neuronal associated[12-15]. They were increased 85, 62, and 49 fold respectively in the LGSI as compared to the PA group. There were several underexpressed transcripts, including a variety of genes encoding extracellular matrix related proteins (e.g. collagens) among others.

Next, we performed immunohistochemistry using commercially available antibodies for routine diagnostic use. Both PA and LGSI demonstrated strong expression of glial markers, including GFAP and S100 protein. In addition, LGSI showed more frequent expression of neuronal-associated markers compared to PA, including synaptophysin (2 of 4 vs. 2 of 6, respectively), chromogranin A (1 of 4 vs. 0 of 5, respec-

Table 1. Ultrastructural features of NF1-associated low grade astrocytomas

Case	Histology	Sex	Age	Location	Rosenthal Fibers	Microtubules	Intermediate Filaments	Dense Core Granules	Organelles	Macro-nucleolus	EGBs
1	PA	F	25	Left lateral ventricle	No	No	Yes	No	Mitochondria	Yes	No
2	PA	M	16	Right parietal	No	No	Yes	No	Mitochondria	No	No
3	PA	M	3	Left optic nerve	Yes	No	Yes	No	Scant Mitochondria	No	No
4	PA	F	21	Temporoparietal lobe	Yes	No	Yes	No	Lysosomes	No	Yes
5	PA	M	2	Left optic nerve	No	No	Yes	No	Lysosomes	No	Yes
6	PA	M	44	Right thalamus and optic	No	Yes	Yes	No	Scant	No	No
7	PA	F	24	Cervicomedullary junction	Yes	No	Yes	No	Mitochondria	Yes	No
8	PA	M	37	brain stem	Yes	No	Yes	No	Lysosomes	Yes	No
9	PA	M	10	Right cerebellum	No	No	Yes	No	Lysosomes and Mitochondria	No	No
10	PA	M	17	Left frontal lobe	No	No	Yes	No	Scant Mitochondria	Yes	No
11	LGSI	M	13	Right temporooccipital	Yes	Yes	Yes	Yes	Mitochondria	Yes	Yes
12	LGSI	F	14	Right subinsular region	No	No	Yes	Yes	Lysosomes and Mitochondria	Yes	Yes
13	LGSI	F	9	Posterior Fossa	Yes	Yes	Yes	Yes	Lysosomes and	No	No
14	DA	F	31	Pons	Yes	No	Yes	No	Mitochondria	No	No
15	GG	M	34	Hypothalmus/3rd ventricle	No	No	Yes	Yes	Lysosomes and Mitochondria	Yes	Yes

PA=Pilocytic astrocytoma; LGSI=low grade astrocytoma subtype indeterminate; DA=diffuse astrocytoma; GG=ganglioglioma; EGBs=eosinophilic granular bodies

Table 2. Clinicopathologic features of NF1-associated low grade astrocytomas with plump cytoplasm and prominent nucleoli

Age/sex	Location	Imaging	surgery	Granular bodies	Rosenthal fibers	Mitotic count/ 10 hpf	Necrosis	Vascular changes	Treatment	Follow-up
46/F	R temporal lobe	Angiogram: large rather avascular mass. Evidence of uncal herniation	STR	absent	absent	1	absent	Glomeruloid and hyalinized vessels	Radiation	Postoperative course complicated by large subgaleal effusion and meningitis, became apneic; probable uncal herniation, expired
64/F	R temporal lobe	CT: enhancing, slightly hyperdense, minimal edema or mass effect	Stereotactic biopsy	present	absent	4	absent	Glomeruloid and hyalinized vessels	NA	Further tx recommended but patient discharged. Died of pneumonia 4 months after surgery
14/F	R insula	MRI: 1.2 cm well circumscribed homegeneouly enhancing lesion, surrounding edema, multiple UBO's	GTR	absent	absent	0	absent	Glomeruloid vessels	Observation	NED 3 years postop
13/M	R temporo-occipital lobe	MRI: 1.5 cm homogeneously enhancing, suggestion that might be arising from the tentorium	GTR	absent	absent	0	absent	Glomeruloid vessels and hyalinized vessels	Observation	NED 40 months postop
9/F	Cerebellum	Well circumscribed inhomogeneously enhancing tumor "most likely extra-axial within the precentral cerebellar sulcus"	Biopsy only	absent	absent	0	absent	Hyalinized vessels	Observation	Stable serial imaging, with follow-up 16 years
4/M	3rd Ventricle	MRI: 1.3 x 1.2 x 0.7 cm, non-enhancing mass involving the posterior aspect of the 3rd ventricle	GTR	absent	absent	1	absent	absent	Observation	Recurrence at 31 months; 2nd GTR performed

Abbreviations: hpf=high power fields; STR=subtotal resection, GTR=gross total resection; NED=no evidence of disease; NA=not available

Table 3. Gene expression analysis of NF1-associated LGSI (n=1) and PA (n=5). Genes expressed ≥ 7 fold in LGSI compared to the PA group

Probe	UniGene ID	Gene Title	Gene Symbol	Fold change LGSI/PA
207014_at	Hs.116250	gamma-aminobutyric acid (GABA) A receptor, alpha 2	GABRA2	85
203999_at	Hs.310545	synaptotagmin I	SYT1	62
204081_at	Hs.524116	neurogranin (protein kinase C substrate, RC3)	NRGN	49
206172_at	Hs.336046	interleukin 13 receptor, alpha 2	IL13RA2	47
204229_at	Hs.375616	solute carrier family 17, member 7	SLC17A7	45
229039_at	Hs.445503	synapsin II	SYN2	43
203649_s_at	Hs.466804	phospholipase A2, group IIA	PLA2G2A	43
202018_s_at	Hs.529517	lactotransferrin	LTF	39
228245_s_at	Hs.524331	ovostatin /// ovostatin 2	OVOS /// OVOS2	33
227053_at	Hs.520087	protein kinase C and casein kinase substrate in neurons 1	PACSIN1	30
204230_s_at	Hs.375616	solute carrier family 17, member 7	SLC17A7	26
210040_at	Hs.21413	solute carrier family 12, member 5	SLC12A5	24
1553605_a_at	Hs.226568	ATP-binding cassette, sub-family A (ABC1), member 13	ABCA13	24
205489_at	Hs.924	crystallin, mu	CRYM	23
204714_s_at	Hs.30054	coagulation factor V (proaccelerin, labile factor)	F5	23
204260_at	Hs.516874	chromogranin B (secretogranin 1)	CHGB	23
206280_at	Hs.317632	cadherin 18, type 2	CDH18	22
203797_at	Hs.444212	visinin-like 1	VSNL1	20
209160_at	Hs.78183	aldo-keto reductase family 1, member C3	AKR1C3	18
212473_s_at	Hs.501928	microtubule associated monoxygenase, calponin and LIM domain containing 2	MICAL2	18
203998_s_at	Hs.310545	synaptotagmin I	SYT1	18
224795_x_at	Hs.703932	immunoglobulin kappa locus	IGK@ /// IGKC	17
205499_at	Hs.306339	sushi-repeat-containing protein, X-linked 2	SRPX2	17
211430_s_at	Hs.700112	immunoglobulin heavy locus	IGH@ /// IGHG1 /// IGHG2 /// IGHM /// IGHV4-31 /// LOC100294459	16
201340_s_at	Hs.104925	ectodermal-neural cortex (with BTB-like domain)	ENC1	15
1565162_s_at	Hs.389700	microsomal glutathione S-transferase 1	MGST1	15
201843_s_at	Hs.76224	EGF-containing fibulin-like extracellular matrix protein 1	EFEMP1	15
228302_x_at	Hs.197922	calcium/calmodulin-dependent protein kinase II inhibitor 1	CAMK2N1	14
228367_at	Hs.628152	alpha-kinase 2	ALPK2	14

226086_at	Hs.436643	synaptotagmin XIII	SYT13	14
202508_s_at	Hs.167317	synaptosomal-associated protein, 25kDa	SNAP25	13
242344_at	Hs.303527	gamma-aminobutyric acid (GABA) A receptor, beta 2	GABRB2	13
224209_s_at	Hs.494163	guanine deaminase	GDA	13
1552714_at	Hs.30917	cellular repressor of E1A-stimulated genes 2	CREG2	13
201341_at	Hs.104925	ectodermal-neural cortex (with BTB-like domain)	ENC1	13
202628_s_at	Hs.414795	serpin peptidase inhibitor, clade E, member 1	SERPINE1	13
221671_x_at	Hs.703932	immunoglobulin kappa locus	IGK@ /// IGKC	13
1555229_a_at	Hs.458355	complement component 1, s subcomponent	C1S	13
223316_at	Hs.498720	coiled-coil domain containing 3	CCDC3	12
213332_at	Hs.187284	pappalysin 2	PAPPA2	12
221651_x_at	Hs.703932	immunoglobulin kappa locus	IGK@ /// IGKC	12
203705_s_at	Hs.173859	frizzled homolog 7 (Drosophila)	FZD7	12
225815_at	Hs.193235	complexin 2	CPLX2	12
238426_at	Hs.270753	transmembrane protein 130	TMEM130	12
223500_at	Hs.478930	complexin 1	CPLX1	11
206552_s_at	Hs.2563	tachykinin, precursor 1	TAC1	11
202733_at	Hs.519568	prolyl 4-hydroxylase, alpha polypeptide II	P4HA2	11
204563_at	Hs.82848	selectin L	SELL	11
202437_s_at	Hs.154654	cytochrome P450, family 1, subfamily B, polypeptide 1	CYP1B1	11
205525_at	Hs.490203	caldesmon 1	CALD1	10
226931_at	Hs.401954	transmembrane and tetratricopeptide repeat containing 1	TMTC1	10
214432_at	Hs.515427	ATPase, Na+/K+ transporting, alpha 3 polypeptide	ATP1A3	10
1553604_at	Hs.226568	ATP-binding cassette, sub-family A (ABC1), member 13	ABCA13	10
205591_at	Hs.522484	olfactomedin 1	OLFM1	9
202435_s_at	Hs.154654	cytochrome P450, family 1, subfamily B, polypeptide 1	CYP1B1	9
229461_x_at	Hs.146542	neuronal growth regulator 1	NEGR1	9
230262_at	Hs.23172	ST8 alpha-N-acetyl-neuraminide alpha-2,8-sialyltransferase 3	ST8SIA3	9
241763_s_at	Hs.403933	F-box protein 32	FBXO32	9
203706_s_at	Hs.173859	frizzled homolog 7 (Drosophila)	FZD7	9
231736_x_at	Hs.389700	microsomal glutathione S-transferase 1	MGST1	9
210016_at	Hs.434418	myelin transcription factor 1-like	MYT1L	9
224918_x_at	Hs.389700	microsomal glutathione S-transferase 1	MGST1	9
226322_at	Hs.401954	transmembrane and tetratricopeptide repeat containing 1	TMTC1	9

211126_s_at	Hs.530904	cysteine and glycine-rich protein 2	CSRP2	8
208051_s_at	Hs.482038	poly(A) binding protein interacting protein 1	PAIP1	8
204463_s_at	Hs.183713	endothelin receptor type A	EDNRA	8
1557122_s_at	Hs.303527	gamma-aminobutyric acid (GABA) A receptor, beta 2	GABRB2	8
223654_s_at	Hs.435976	bruno-like 4, RNA binding protein (Drosophila)	BRUNOL4	8
201842_s_at	Hs.76224	EGF-containing fibulin-like extracellular matrix protein 1	EFEMP1	8
230303_at	Hs.648668	synaptoporin	SYNPR	8
203798_s_at	Hs.444212	visinin-like 1	VSNL1	8
206190_at	Hs.46453	G protein-coupled receptor 17	GPR17	8
204723_at	Hs.4865	sodium channel, voltage-gated, type III, beta	SCN3B	8
204339_s_at	Hs.386726	regulator of G-protein signaling 4	RGS4	8
229331_at	Hs.527090	spermatogenesis associated 18 homolog (rat)	SPATA18	7
203305_at	Hs.335513	coagulation factor XIII, A1 polypeptide	F13A1	7
214920_at	Hs.648482	thrombospondin, type I, domain containing 7A	THSD7A	7
207030_s_at	Hs.530904	cysteine and glycine-rich protein 2	CSRP2	7
212792_at	Hs.408623	dpy-19-like 1 (C. elegans)	DPY19L1	7
205110_s_at	Hs.6540	fibroblast growth factor 13	FGF13	7
235066_at	Hs.517949	microtubule-associated protein 4	MAP4	7
204684_at	Hs.702002	neuronal pentraxin I	NPTX1	7
201616_s_at	Hs.490203	caldesmon 1	CALD1	7
218084_x_at	Hs.333418	FXYD domain containing ion transport regulator 5	FXYD5	7
205876_at	Hs.133421	leukemia inhibitory factor receptor alpha	LIFR	7
204337_at	Hs.386726	regulator of G-protein signaling 4	RGS4	7
213131_at	Hs.522484	olfactomedin 1	OLFM1	7
204722_at	Hs.4865	sodium channel, voltage-gated, type III, beta	SCN3B	7
220131_at	Hs.134729	FXYD domain containing ion transport regulator 7	FXYD7	7
221914_at	Hs.225936	synapsin I	SYN1	7
201266_at	Hs.708065	thioredoxin reductase 1	TXNRD1	7
204035_at	Hs.516726	secretogranin II (chromogranin C)	SCG2	7

Table 4. Summary of immunohistochemical analysis for glial and neuronal markers in LGSI and PA

N	LGSI n=4	PA n=6
GFAP	4 (of 4)	6 (0f 6)
S100	4 (of 4)	ND
Synaptophysin	2 (of 4)	2 (of 6)
Chromogranin	1 (of 4)	0 (of 5)
Neurofilament protein	2 (of 4)	0 (of 4)

tively), and neurofilament protein (2 of 4 vs. 0 of 4, respectively) (**Figure 3** and **Table 4**). The two LGSI expressing neurofilament protein in tumor cells also expressed synaptophysin. In the 2 PA expressing synaptophysin, it was limited to rare cells. The GG showed strong expression of synaptophysin and chromogranin in the neuronal component. Partial infiltration of underlying brain parenchyma was noted in 5 (of 6) PA and 3 (of 4) LGSI. These findings support a predominantly glial and partial neuronal phenotype for NF1-associated LGSI compared with PA.

A subset of NF1-associated low grade astrocytomas demonstrate increased mTOR pathway activation

Given the increased cytoplasmic size and the presence of macronucleoli in the LGSI group, we hypothesized that increased mTOR signaling may partially explain this phenotype. We performed western blot analysis using an antibody recognizing phospho-S6, a marker reflecting mTOR activation. Increased levels of phospho-S6 were present in 3 NF1-associated low grade astrocytomas (1 LGSI and 2 PA) compared to cerebral cortex and cerebellum, levels being highest in the LGSI, when adjusting for beta actin or total S6 (**Figure 4**).

Next we performed immunohistochemistry using antibodies recognizing phospho-S6 and phospho-p70S6K in formalin-fixed paraffin-embedded tissue. Immunopositivity for both was noted in 7 (of 12) and 5 (of 13) PA and 4 (of 4) of LGSI each respectively (**Figure 5**). Combined immunoreactivity for phospho-S6 and phospho-p70S6K was noted in 5(of 13) of PA and 4 (of 4) LGSI, the difference being statistically significant (p=0.02) (Fisher exact test). To assess the status of mTOR activation in additional non-NF1 associated tumors, we also performed immunohistochemistry using two tissue microarrays including sporadic tumors. Combined immunopositivity for phospho-S6 and phospho-p70S6K was demonstrated in 13 (of 39)(33%) sporadic PA.

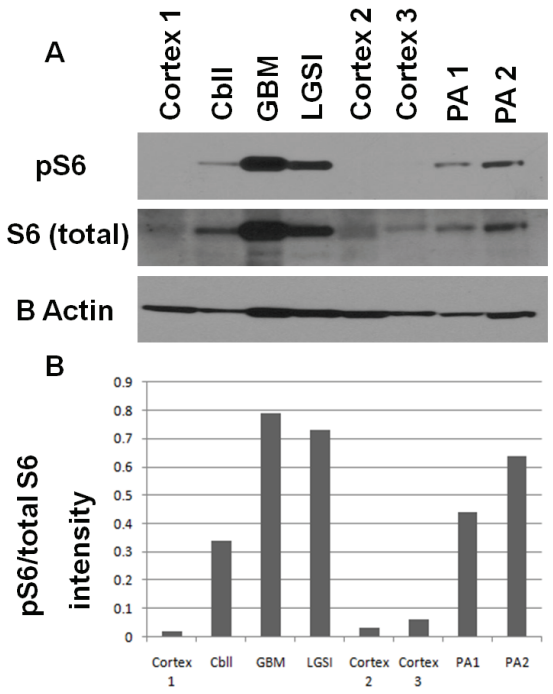

Figure 4. Increased phospho-S6 levels are a feature of low grade astrocytomas subtype indeterminate (LGSI). One case of LGSI tested showed a strong band when using an anti phospho-S6 antibody (A). When quantifying relative band intensity using ImageJ software, there was 12-40% increased levels in the LGSI compared to two NF1-associated PA. Levels were adjusted for total S6 to control for gel loading. CbII=cerebellum, GBM=Glioblastoma sample control, cortex=non-neoplastic cerebral cortex.

In contrast there were no differences with respect to phospho-ERK immunoreactivity, which was uniformly expressed in all NF1-associated PA and LGSI, or in MIB1 labeling (mean MIB1 3.2 and 5 respectively, p=0.2). *BRAF* duplication was absent in 8 NF1-associated low grade astrocytomas, including 7 PA and 1 LGSI. When reviewing gene expression data focusing on mTOR target genes, the results were variable and difficult to interpret, with some genes showing increased expression and some decreased expression in the single LGSI compared to the NF1-associated PA. Genes overexpressed 2-3 fold in the LGSI included those encoding for

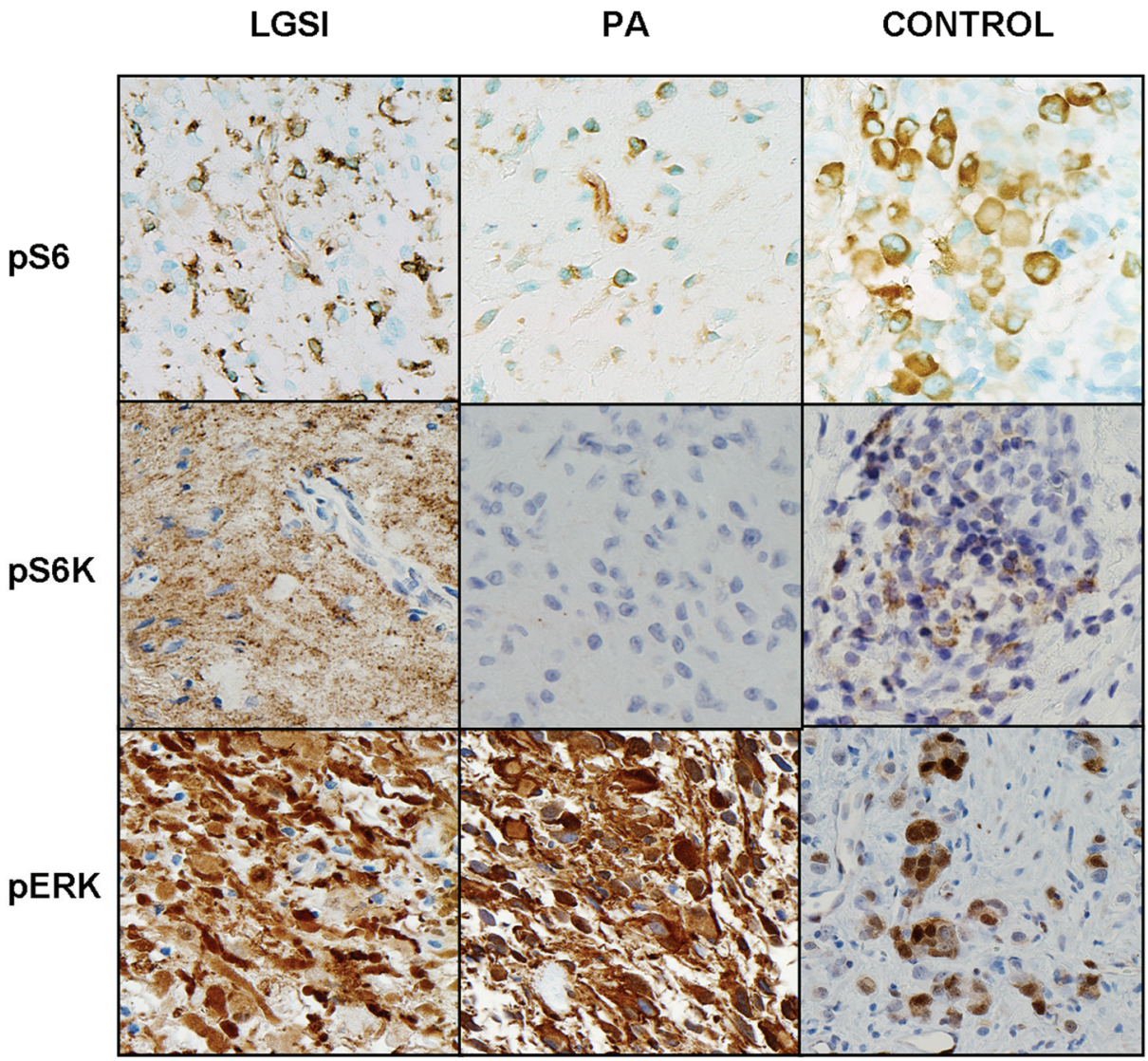

Figure 5. Increased frequency of combined phospho-S6/phospho-S6 kinase is present in low grade astrocytomas subtype indeterminate (LGSI). Using immunohistochemistry for phospho-S6 and phospho-S6 kinase, combined immunoreactivity was present in all LGSI tested (4), but in less than half of PA.

eukaryotic translation initiation factor 4E, eukaryotic translation initiation factor 3, subunit B, and RHEB. These findings suggest that increased mTOR signaling, but not MAPK/ERK activation or proliferation, may underlie the phenotypic variations noted in NF1-associated low grade astrocytomas.

Discussion

NF1 associated low grade astrocytomas are predominantly pilocytic in type. Prior studies have indicated that a subset of low grade astrocytomas are difficult to classify, but offer no explanation of phenotypic variations in terms of possible underlying molecular mechanisms. As would be expected, the most conspicuous ultrastructural finding within all tumors in this study was the presence of numerous intermediate filaments, typical of astrocytic neoplasms. In our study, the majority of tumors available for ultrastructural review were PA. Most demonstrated typical features one would expect, such as Rosenthal fibers and intermediate filaments. In

the GG intermediate filaments were present only within phenotypically glial cells. As expected, dense core granules were abundantly present in the GG, but were also sparsely represented in all three LGSI examined. Rosenthal fibers not appreciated on light microscopy were present ultrastructurally in LGSI as well as the single diffuse astrocytoma, thus suggesting morphologic similarities, at least at the ultrastructural level, among all low grade astrocytomas in NF1. Instead, the presence of ultrastructural features usually associated with a neuronal phenotype, including aligned microtubules and dense core granules, was typical, albeit an unexpected feature, of LGSI. These findings within low grade astrocytomas may represent phenotypic divergent differentiation in the setting of NF1.

A partial neuronal phenotype was also demonstrated by gene expression analysis (in a single tumor) and by increased expression of neuronal markers at the protein level. However, the predominant line of differentiation of these tumors remains glial, as reflected by strong consistent GFAP immunoreactivity and intermediate filament accumulation in all tumors. Classic neuronal and glioneuronal tumors have also been described in the setting of NF1, including gangliogliomas [1, 16], DNET like lesions [16] and even desmoplastic infantile gangliogliomas [1]. Unlike these lesions, our LGSI subset exhibits a predominant glial phenotype with only partial divergent neuronal differentiation, as described in other astrocytomas, including subependymal giant cell astrocytoma and pleomorphic xanthoastrocytoma [17, 18].

The morphology of this low grade astrocytoma subset is somewhat reminiscent of another syndrome-associated tumor, i.e. subependymal giant cell astrocytoma. The features include nucleolar prominence, abundance of cytoplasm, expression of neuronal markers, and favorable prognosis [18]. Subependymal giant cell astrocytoma is nearly restricted to patients with tuberous sclerosis, a syndrome arising as a consequence of *TSC1* or *TSC2* germline mutations. The molecular consequence is activation of the mTOR pathway [10]. mTOR activation may also be an important biological event in epilepsy associated glioneuronal tumors [19].

Increased mTOR activation has been shown to occur in NF1 deficient astrocytes and in 4 of 6 NF1-associated PA in a prior study [8]. Curiously, in our group of NF1-associated low grade astrocytomas mTOR activation, as reflected by phospho-S6 and phospho-p70S6K levels, was frequent, but seemed to be higher in the low grade astrocytomas with peculiar cytologic features. Phospho-S6 levels are increased as a result of activation of mTOR which leads to phosphorylation of p70S6 kinase and thus activation of ribosomal S6, which leads to increased protein synthesis. The result may be increased cell size. These findings support the notion that some low grade astrocytomas represent a distinct morphologic subset of NF1-associated tumors. Although no obvious clinical differences are noted with respect to NF1-associated PA, our findings could be clinically relevant since the mTOR pathway may be pharmacologically targeted for therapeutic benefit [20].

MAPK/ERK activation, as demonstrated by phospho-ERK immunoreactivity, was uniform in all tumors studied. This is expected, given that NF1 loss results in persistent activated RAS and downstream signaling through the MAPK/ERK pathway[8]. *BRAF* rearrangements and mutations represent an alternative mechanism of MAPK/ERK activation in sporadic PA [21]. It is of interest that prior studies have found *BRAF* alterations to be absent in NF1-associated astrocytomas [22, 23], including 7 PA and 1 LGSI used in the current study. Therefore, *BRAF* testing is not useful in distinguishing these subtypes of low grade astrocytoma in the setting of NF1.

One caveat is that not all LGSI demonstrate this unique morphology, and some may in fact represent other, inadequately sampled histologies, such as PA [1]. Indeed, the possibility of undersampling resulting in an erroneous diagnosis is a consideration whenever tumors with overlapping morphologic and ultrastructural features are encountered.

Our study suggests that NF1-associated PA and LGSI share some phenotypic features at the ultrastructural level, particularly Rosenthal fiber formation. However, the presence of occasional dense core granules and microtubules in addition to increased expression of neuronal associated genes, may represent divergent differentiation of some low grade astrocytomas in comparison with classic PA, the most prototypic NF1

associated astrocytoma. Furthermore, increased mTOR activation may be responsible for larger cell size despite similar proliferative indices and clinical behavior. Our findings, perhaps underlying the unconventional morphology of these tumors, require further studies to shed light upon the biology and molecular mechanisms underlying NF1-associated glial tumorigenesis.

Acknowledgments

The authors thank the microarray, cytogenetics, tissue and cell molecular analysis of the Mayo Clinic for excellent technical assistance.

This work was funded in part by grant P50 CA108961 from the Mayo SPORE in Brain Cancer (CG, FJR, JNS) and Mayo Clinic CTSA (FJR) through grant number UL1 RR024150 from the National Center for Research Resources (NCRR), a component of the National Institutes of Health (NIH).

Please address correspondence to: Fausto J. Rodriguez MD, Department of Pathology, Division of Neuropathology, Johns Hopkins University, 720 Rutland Avenue - Ross Building - 512B, Baltimore, Maryland 21205, USA. Tel: 443-287-6646; Fax: 410-955-9777, E-mail: frodrig4@jhmi.edu

References

[1] Rodriguez FJ, Perry A, Gutmann DH, O'Neill BP, Leonard J, Bryant S, Giannini C. Gliomas in neurofibromatosis type 1: a clinicopathologic study of 100 patients. J Neuropathol Exp Neurol 2008; 67: 240-249.

[2] Liberski PP, Kordek R. Ultrastructural pathology of glial brain tumors revisited: a review. Ultrastruct Pathol 1997; 21: 1-31.

[3] Luse SA. An electron microscopic study of normal optic nerve and of an optic-nerve glioma. J Neurosurg 1961; 18: 466-478.

[4] Soejima T, Kitamura K, Tomonaga M. [Electron microscopic observation of optic glioma--with special reference to the desmoplastic reaction (author's transl)]. No Shinkei Geka 1974; 2: 689-697.

[5] Stern J, Jakobiec FA, Housepian EM. The architecture of optic nerve gliomas with and without neurofibromatosis. Arch Ophthalmol 1980; 98: 505-511.

[6] Kim KY, Ju WK, Hegedus B, Gutmann DH, Ellisman MH. Ultrastructural characterization of the optic pathway in a mouse model of neurofibromatosis-1 optic glioma. Neuroscience 170: 178-188.

[7] Scheithauer BW, Bruner JM. The ultrastructural spectrum of astrocytic neoplasms. Ultrastruct Pathol 1987; 11: 535-581.

[8] Dasgupta B, Yi Y, Chen DY, Weber JD, Gutmann DH. Proteomic analysis reveals hyperactivation of the mammalian target of rapamycin pathway in neurofibromatosis 1-associated human and mouse brain tumors. Cancer Res 2005; 65: 2755-2760.

[9] Gingras AC, Raught B, Sonenberg N. Control of translation by the target of rapamycin proteins. Prog Mol Subcell Biol 2001; 27: 143-174.

[10] Chan JA, Zhang H, Roberts PS, Jozwiak S, Wieslawa G, Lewin-Kowalik J, Kotulska K, Kwiatkowski DJ. Pathogenesis of tuberous sclerosis subependymal giant cell astrocytomas: biallelic inactivation of TSC1 or TSC2 leads to mTOR activation. J Neuropathol Exp Neurol 2004; 63: 1236-1242.

[11] Rodriguez FJ, Giannini C, Asmann YW, Sharma MK, Perry A, Tibbetts KM, Jenkins RB, Scheithauer BW, Anant S, Jenkins S, Eberhart CG, Sarkaria JN, Gutmann DH. Gene expression profiling of NF-1-associated and sporadic pilocytic astrocytoma identifies aldehyde dehydrogenase 1 family member L1 (ALDH1L1) as an underexpressed candidate biomarker in aggressive subtypes. J Neuropathol Exp Neurol 2008; 67: 1194-1204.

[12] Enna SJ, McCarson KE. The role of GABA in the mediation and perception of pain. Adv Pharmacol 2006; 54: 1-27.

[13] Mikoshiba K, Fukuda M, Ibata K, Kabayama H, Mizutani A. Role of synaptotagmin, a Ca2+ and inositol polyphosphate binding protein, in neurotransmitter release and neurite outgrowth. Chem Phys Lipids 1999; 98: 59-67.

[14] Mirza NR, Munro G. The role of GABA(A) receptor subtypes as analgesic targets. Drug News Perspect 23: 351-360.

[15] Zhong L, Cherry T, Bies CE, Florence MA, Gerges NZ. Neurogranin enhances synaptic strength through its interaction with calmodulin. Embo J 2009; 28: 3027-3039.

[16] Fedi M, Anne Mitchell L, Kalnins RM, Gutmann DH, Perry A, Newton M, Brodtmann A, Berkovic SF. Glioneuronal tumours in neurofibromatosis type 1: MRI-pathological study. J Clin Neurosci 2004; 11: 745-747.

[17] Giannini C, Scheithauer BW, Lopes MB, Hirose T, Kros JM, VandenBerg SR. Immunophenotype of pleomorphic xanthoastrocytoma. Am J Surg Pathol 2002; 26: 479-485.

[18] Lopes MB, Altermatt HJ, Scheithauer BW, Shepherd CW, VandenBerg SR. Immunohistochemical characterization of subependymal giant cell astrocytomas. Acta Neuropathol 1996; 91: 368-375.

[19] Boer K, Troost D, Timmermans W, van Rijen PC, Spliet WG, Aronica E. Pi3K-mTOR signaling and AMOG expression in epilepsy-associated glioneuronal tumors. Brain Pathol 20: 234-244.

[20] Franz DN, Leonard J, Tudor C, Chuck G, Care M,

Sethuraman G, Dinopoulos A, Thomas G, Crone KR. Rapamycin causes regression of astrocytomas in tuberous sclerosis complex. Ann Neurol 2006; 59: 490-498.

[21] Jones DT, Kocialkowski S, Liu L, Pearson DM, Backlund LM, Ichimura K, Collins VP. Tandem duplication producing a novel oncogenic BRAF fusion gene defines the majority of pilocytic astrocytomas. Cancer Res 2008; 68: 8673-8677.

[22] Rodriguez EF, Scheithauer BW, Giannini C, Rynerason A, Cen L, Hoesley B, Gilmer-Flynn H, Sarkaria JN, Jenkins S, Long J, Rodriguez FJ. PI3K/AKT Pathway Alterations are Associated With Clinically Aggressive and Histologically Anaplastic Subsets of Pilocytic Astrocytoma. Acta Neuropathol 2010.

[23] Zeng N, Liu L, McCabe MG, Jones DT, Ichimura K, Collins VP. Real-time quantitative polymerase chain reaction (qPCR) analysis with fluorescence resonance energy transfer (FRET) probes reveals differential expression of the four ERBB4 juxtamembrane region variants between medulloblastoma and pilocytic astrocytoma. Neuropathol Appl Neurobiol 2009; 35: 353-366.